NIPER-496
October 1990

NIPER
Commitment to Excellence

TOPICAL REPORT

RELATIVE PERMEABILITIES AND OTHER CHARACTERISTICS OF 700-MILLIDARCY, FIRED BEREA SANDSTONE

by

D.R. Maloney, A.D. Brinkmeyer, and M.M. Honarpour

Work Performed for the
U.S. Department of Energy
Under Cooperative Agreement DE-FC22-83FE60149

National Institute for Petroleum and Energy Research
IIT Research Institute • P.O. Box 2128
Bartlesville, Oklahoma 74005 • (918) 336 - 2400

NIPER-496
Distribution Category UC-122
October 1990

Topical Report

RELATIVE PERMEABILITIES AND OTHER CHARACTERISTICS OF 700-MILLIDARCY, FIRED BEREA SANDSTONE

By

D. R. Maloney, A. D. Brinkmeyer, and M. M. Honarpour

Project BE9, Milestone 4, FY90

Work Performed for
U. S. Department of Energy
Under Cooperative Agreement
DE-FC22-83FE60149

Edith Allison
Project Manager
Bartlesville Project Office
U. S. Department of Energy
Bartlesville, Oklahoma

DISCLAIMER

IIT Research Institute
NATIONAL INSTITUTE FOR PETROLEUM AND ENERGY RESEARCH
P. O. Box 2128
Bartlesville, OK 74005

TABLE OF CONTENTS

Page

Abstract 1

Introduction 1

Experimental procedures and measurements 3
Sample characterization 4
Capillary pressure and wettability measurements 4
Amott tests 4
Centrifuge capillary pressure tests 5
Relative permeability measurements 6
Oil-water tests 6
Gas-water tests 7
Three-phase tests 7

Results 7
Sample physical characteristics 7
Clay and minerals 7
Pore and grain size distributions 8
Fluid characteristics 8
Capillary pressure and wettability 9
Amott tests 9
Centrifuge capillary pressure tests 9
Relative permeability measurements 11
Oil-water 11
Gas-water 12
Three-phase 12

Discussion 12
Capillary pressure/wettability measurements 12
Comparison of two-phase results from this investigation 13
Comparison of two-phase results with those from other investigations 13

Conclusions 14

Acknowledgments 15

References 16

Appendix A - Temperature experiments 33
Appendix B - New equipment and automation 35

TABLES

1. Characteristics of the 700-md fired Berea sandstone sample from routine core analysis and mercury intrusion porosimetry 18

2. Log-normal distribution function characteristics for Bentheimer and Berea sandstones 18

3. Characteristics of the brine and oil used in centrifuge capillary pressure and imbibition tests 18

4. Wettability indices calculated from 700-md Berea capillary pressure results 18

5. Unsteady-state oil-water relative permeability results for Berea plugs 1 and 2 19

TABLES (Continued)

Page

6. Unsteady-state oil-water results for Berea sandstone plug 3 20

7. Oil-water relative permeability and resistivity data for sample 5 (700-md fired Berea) 21

8. Sample 5 oil-water resistivity results 22

9. Sample B72 gas-water data 23

10. Sample 6 gas-water resistivity results 24

ILLUSTRATIONS

1. Dimensions and electrode layout for rectangular samples 4, 5, and 6 25

2. X-ray diffraction bulk and clay analyses, 700-md fired Berea 25

3. Grain diameter distributions for fired Bentheimer and Berea samples from thin-section analyses 26

4. Pore diameter distributions for fired Bentheimer and Berea samples from thin-section analyses 26

5. Mercury intrusion porosimetry results for Bentheimer and Berea samples 27

6. CT images of the 700-md Berea during the 1st imbibition (left side) and 2nd drainage cycles showing brine (light) and oil (dark) distributions 27

7. Steady-state oil water results for sample 4 (2,000-mdBerea sandstone). 28

8. Unsteady-state relative permeability results for 700-md Berea sandstone plugs 1, 2, and 3 28

9. Steady-state oil-water relative permeability results for sample 5 (700-md fired Berea) 29

10. Resistivity index results measured during the steady-state oil-water test on sample 5 29

11. Sample 5 resistivity index results showing curve fits and saturation exponents ('n') 30

12. Steady-state gas-water relative permeability results for sample 6 (700-md fired Berea) 30

13. Sample 6 resistivity index results from measurements during steady-state gas-water tests 31

14. Two-phase graphs of water, oil (water-oil imbibition), and gas (gas-liquid drainage) 31

15. Model curves interpreted from model results. 32

B-1. Generalized schematic of the input/output interconnections among the laboratory devices and measurement and control systems 36

RELATIVE PERMEABILITIES AND OTHER CHARACTERISTICS OF 700-MILLIDARCY, FIRED BEREA SANDSTONE

By

D. R. Maloney, A. D. Brinkmeyer, and M. M. Honarpour

ABSTRACT

A laboratory investigation was conducted to determine the petrophysical, capillary pressure, and relative permeability characteristics of a 700-md fired Berea sandstone. Thin section analyses, CT scans, mercury injection porosimetry, centrifuge capillary pressure, and spontaneous imbibition tests were used as aids in characterizing pore and grain size distributions, capillary pressures, wettability indices, and fluid distributions. Cycle-dependent capillary pressure and relative permeability behavior for the sample were evaluated during the experimental program. Relative permeability experiments conducted on samples of the rock included two-phase, unsteady-state oil-water tests, steady-state oil-water and steady-state gas-water tests, and three-phase steady-state tests. Resistivity characteristics also were measured during the steady-state relative permeability tests. Relative permeability and resistivity results are reported in both graphical and tablular forms. These FY89 Berea sandstone results provide data for comparing relative permeabilities and other rock characteristics of this sample with those of higher permeability (2 darcy range) tested during FY88.

Hysteresis was evident in the results from each multiple-cycle capillary pressure experiment. The primary effect of cycle-dependent capillary pressure changes for these samples was a reduction in the wettability index with successive drainage and imbibition cycles. The data for capillary pressures lower than 3 psi were very repeatable and did not appear to be affected by hysteresis. Fluid distributions during centrifuge tests were nonuniform except for saturations near the residual oil or water conditions. Discernable hysteresis effects in the two-phase relative permeability results essentially were limited to the nonwetting phase relative permeability versus saturation curves between the first drainage and imbibition tests. Wetting phase relative permeability characteristics were consistent throughout. Comparisons among unsteady- and steady-state relative permeability results from this investigation as well as some comparisons with work of other investigators are presented.

INTRODUCTION

Relative permeability data accurately depicting multiphase flow effects are frequently required for reservoir engineering calculations. Considerations often include the displacement of oil by simultaneous gas and water flow and an estimation of the volume of oil recovered as well as that left in place after primary and secondary production. Enhanced recovery processes also involve three-phase flow in which one of the flowing phases is injected to modify reservoir behavior and to improve petroleum production.

Current reservoir engineering practices include the use of numerical simulators to predict reservoir performance. The appropriateness of the output from a numerical simulator in modeling reservoir performance is directly related to the quality of the data or correlations, representing fluid flow characteristics, entered into the simulator. In the absence of correlations from three-phase relative permeability test data, three-phase flow characteristics are generally determined from more readily available two-phase gas-oil and water-oil data. However, two-phase flow characteristics may not represent three-phase characteristics adequately. For these reasons, it is important to understand three-phase flow processes and to develop correlations and predictive methods for modeling relative permeabilities under multiphase flow conditions. Knowledge of three-phase relative permeability and flow behavior is especially useful to smaller companies, without extensive laboratory facilities, for use in publicly available reservoir simulators.

Various factors influence multiphase relative permeability characteristics. Several studies have shown the relationship between capillary number and two-phase relative permeability. Fluid velocity, interfacial tension, and viscosity effects on two-phase relative permeability have been studied to some extent, and guidelines for producing quality data for two-phase flow tests have been recommended. However, guidelines or studies showing the effect of rock, fluid, and rock-fluid properties and hysteresis on relative permeabilities are scarce.

The limited results reported for three-phase flow characteristics have shown that the fluid saturation envelope for three-phase flow is narrow and is affected by rock properties, wettability, and hysteresis among other factors. Since rock and wettability properties are responsible for cycle-dependent hysteresis in relative permeability characteristics, an understanding of the relationships among the three is important. Cycle-dependent hysteresis has significant implications on reservoir performance prediction. In the process of waterflooding a water-wet reservoir, the rock in front of the oil bank experiences a drainage process (water saturation decreasing) as the oil bank moves towards production wells. The rock behind the oil bank experiences an imbibition process (water saturation increasing). After the oil bank reaches production wells, the reservoir rock undergoes additional drainage and imbibition cycles as oil production continues. Each cycle may yield different relative permeability characteristics which are manifested as hysteresis. Any changes in flooding patterns or profile modification, infill drilling, or application of EOR processes subject the rock to additional hysteresis cycles. The coring, cleaning, and handling of rock samples obtained from the reservoir are often accompanied by one or more hysteresis cycles. Knowledge of the extent of variation in relative permeabilities due to hysteresis provides guidelines for adjusting or using representative relative permeability data in reservoir simulators. Before an understanding of multiphase flow phenomena can be attained, high-quality three-phase flow data recorded under characteristic reservoir conditions must be obtained.

Capillary pressure information is used in a variety of petroleum engineering calculations. The accuracies of reservoir simulations are dependent on the quality of the data used. Accurate laboratory measurements of capillary pressure are important, as documented by Anderson[1,2] and emphasized by Hawkins and Bouchard.[3]

Limited studies have been conducted to investigate capillary pressure/saturation hysteresis effects. Several studies have touched upon the question of the magnitudes and effects of hysteresis on centrifuge capillary pressure/saturation data, such as those by Evrenos and Comer,[4] Szabo,[5] Batycky et al.,[6] and Longeron et al.[7] Others have investigated the influence of reservoir or experimental conditions on hysteresis such as the temperature studies of Sinnokrot et al.[8] and Sanyal et al.[9] Several studies have suggested that wettability and/or pore size distribution are responsible for capillary pressure/saturation hysteresis.

The major objectives of this project were concentrated in two primary areas: examination of mutual relationships among petrophysical properties, rock-fluid characteristics, and relative permeabilities; and improvement in three-phase permeability measurements. Some of the results of this project related to capillary pressure and wettability were presented at a national symposium.[10]

EXPERIMENTAL PROCEDURES AND MEASUREMENTS

A Berea sandstone was selected as the rock material for this investigation. The absolute permeability of the sample was in the 500 to 700 md range, which is about 70% less than the permeabilities of the Berea and Bentheimer sandstones previously characterized.[11] The new sample was selected to be similar to those samples with respect to mineralogy but slightly different with respect to porosity, permeability, and pore and grain shape, size, and number distribution characteristics.

All tests in this investigation were conducted on fired rock samples. The samples were fired in a 1,000° C oven for 24 hr to stabilize clay minerals. Samples of the Berea were prepared for thin sections, X-ray diffraction (XRD), and bulk and clay analyses. Additional samples were cut for use in mercury injection capillary pressure evaluations, centrifuge capillary pressure and wettability tests, and relative permeability experiments. Plugs of 3.8 cm diameter and length were cut for centrifuge capillary pressure tests. These plugs were marked with orientation lines to permit the samples to be oriented correctly during centrifuge experiments. Plugs of 2.5 cm diameter and length were cut for mercury injection porosimetry tests. Plugs for unsteady-state relative permeability tests were of 3.8 cm diameter by 7.6 cm length. Samples with 15 cm lengths and 2.5 cm by 5.1 cm rectangular cross sections were prepared for steady-state relative permeability tests. Current and potential electrodes were affixed to these 15 cm long samples to provide a means for obtaining resistance measurements during the tests. Shallow grooves were cut in the samples

at positions shown in figure 1. The grooves were painted with silver conducting paint, then a wrap of copper wire was placed in each groove. The copper wire was soldered into the groove to provide excellent electrical contact with the sample. The steady-state test samples were jacketed with epoxy resin.

The tests described in this report were conducted at 25° C. Nitrogen was used as the gas phase in relative permeability measurents involving gas as one of the flowing phases. Unless noted otherwise, the test fluids used brine (1 wt % NaCl in water) and Soltrol 100, an isoparaffinic oil available from Phillips Petroleum Company. For steady-state relative permeability tests in which X-ray techniques were used for saturation measurements, the oil was tagged with 10 wt % iododododecane. Brine and water are used synonymously within this report to describe a brine consisting of 1 wt % NaCl in deionized water.

Sample Characterization

Pore and grain size distributions for the fired rock were characterized first by microscopic image analysis. The system consists of of a Dage MTI camera mounted on a Nikon light microscope. Output from the camera is interfaced with a microcomputer. The microcomputer digitizes the images and performs various petrographic measurements and calculations. Features with dimensions in the submicron range were ignored in microscopic grain and pore size number distribution calculations due to microscopic resolution limitations. Five hundred pores and 500 grains were measured by evaluating thin sections with the aid of a microscopic image analysis system.

Mercury intrusion porosimetry tests were conducted on a plug of the sandstone to further characterize its pore size distribution. Volume and pressure measurements from tests in which mercury was forced into the rock pores at pressures from 3.45 kPa to 413 MPa were used to calculate pore diameters and mercury intrusion data.

Capillary Pressure and Wettability Measurements

Spontaneous imbibition and centrifuge capillary pressure tests were conducted on samples of the 700-md fired Berea as well as samples of the higher permeability Berea and Bentheimer sandstones that were characterized last year. Test procedures and results were previously reported.[10] The test fluids consisted of 0.973-cP brine (1 wt % NaCl in water) and a 1.2-cP isoparaffinic oil. The following paragraphs describe the tests that were performed to determine the capillary pressure characteristics and wetting tendencies for the samples.

Amott Tests

Plugs at residual water saturation conditions were placed in brine-filled Amott cells. The volumes of oil drained from the plugs were measured over a 10-day period. Tests were also conducted with plugs

containing residual oil saturations that were placed in oil-filled Amott cells in the same manner. Additional tests were conducted to monitor the fluid distributions as the rocks imbibed brine using a CT scanner.

Centrifuge Capillary Pressure Tests

Each plug was wrapped circumferentially with Teflon tape. The jacket of Teflon tape was used in an effort to prevent radial fluid transfer and to minimize fluid loss from handling. Each plug was marked for reorientation. The first step in each centrifuge capillary pressure test was to saturate the plugs with brine using procedures recommended by Worthington.[12] Pore volumes were calculated from both gas expansion (Boyle's law) and weight-change methods.

High RPM, Long-Term Tests

Brine-saturated plugs were placed in drainage tubes under oil and were centrifuged at nine rotational speeds from 400 to 4,000 RPM. Each speed was maintained for 48 hr before recording the final displaced brine volumes. After completing the first drainage cycle, the plugs were placed under brine in imbibition tubes. Measurements of displaced oil were recorded at centrifuge speeds and times similar to those from the drainage test. Tests continued with second drainage, second imbibition, and third drainage cycles.

Low RPM Tests

Short-term (1 hr/point) and long-term (48 hr/point) centrifuge tests were conducted at centrifuge speeds from 200 to 1,500 RPM. The low RPM tests were conducted because the excessive capillary pressures induced during high RPM tests were suspected of driving residual saturations to values less than those that would be expected during a linear flow test.

Centrifuge/CT Scan Tests

These tests were used to evaluate fluid distributions during centrifuge capillary pressure measurements. A Siemens Somatom 2 CT Scanner was used for CT imaging. CT power settings were 125 kV, 460 mAs. Imaging resolution was about 500 μm. Plugs were CT scanned in their dry and 100% brine saturated conditions initially. Additional scans were taken of the samples during the drainage process. After each measurement, they were centrifuged for 48 hr at speeds of 120, 130, 140, 150, 200, 300, 400, 800, 1,000, 1,200, and 1,500 RPM. Similar procedures were used during the imbibition cycle. For these CT scan tests, the brine was tagged with 10 wt % KBr to provide a high X-ray attenuation contrast between the oil and brine on CT scan images.

Data from the centrifuge capillary pressure tests (displaced fluid volumes, centrifuge rotational speed, rotor radius for drainage, and imbibition) and rock and fluid characteristics were used to construct capillary pressure versus saturation curves and to calculate wettability indices. Most of the capillary

pressure-saturation relationships were determined using both the Hassler-Brunner[13] and Rajan[14] methods, and all of the results were analyzed by the Rajan method. Wettability indices were calculated using the USBM technique.[15]

Relative Permeability Measurements

Samples used for relative permeability tests were designated 1 through 6. Plugs 1, 2, and 3 were of 3.8 cm diameter by 7.6 cm length. Samples 4, 5, and 6 had 15 cm lengths and 2.5 cm by 5.1 cm rectangular cross sections. Care was taken in each relative permeability experiment to control saturation histories.

Oil-Water Tests

Relative permeability hysteresis effects were initially evaluated during a two-phase water-oil relative permeability test conducted on sample 4 (2,000-md Berea sandstone) that was characterized previously.[11] Permeability and saturation measurements were taken as the rock was subjected to multiple drainage and imbibition cycles. In the context of this report for water-wet sandstones, drainage occurs as the wetting phase saturation (water) decreases while imbibition occurs as the wetting phase saturation increases. The 1.4-cP oil was tagged with 10 wt % iodododecane.

Unsteady-state oil-water tests using 0.973-cP brine and a 23.5-cP mineral oil were conducted on plugs 1 and 2. Each sample was initially saturated with brine. The samples were confined at 5.52 MPa confining pressure within a coreholder. The samples were oil-flooded to residual brine saturation conditions, then unsteady-state measurements were recorded as the samples were flooded with brine to residual oil saturation.

Sample 3 was tested under a confining pressure of 2.41 MPa using brine and 93.5-cP oil. Test techniques were similar to those used for plugs 1 and 2, except that after completing an unsteady-state test on the plug, the sample was oil flooded back to residual water saturation and a second unsteady-state test was conducted. Average saturations were determined by volumetric balance methods. The JBN[16] method was used for unsteady-state relative permeability calculations.

Another steady-state oil-water relative permeability experiment was performed on sample 5 (700-md Berea sandstone) using 1-cP brine (1wt % NaCl in water) and 1.4-cP oil tagged with 10 wt % iodododecane (X-ray tag). Effluent pH and four-electrode resistance measurements were taken as the rock was initially flooded with brine of 7.3 pH . Oil and brine permeabilities were measured for two drainage and two imbibition cycles. Resistance, permeability, X-ray, and microwave scan measurements were recorded throughout the test. Saturations were determined using calibration equations relating X-ray and microwave absorption to fluid saturations. For each steady-state saturation measurement, X-ray

scans were taken for tube potential and current settings of 45 kV/10 mA using a tungsten target X-ray tube.

Gas-Water Tests

Steady-state gas-water tests were conducted on sample 6. Saturations were calculated using X-ray and microwave scan data. Relative permeability and resistance measurements were recorded at various gas-to-water flow ratios for two drainage cycles and one imbibition cycle.

Three-Phase Tests

Three-phase relative permeability tests were conducted on sample 6 for several primary drainage (DDI - water saturation decreasing, oil saturation decreasing, and gas saturation increasing) and imbibition (IID - water and oil saturations increasing and gas saturation decreasing) saturation cycles. The rock was initially completely saturated with brine. Two phase oil-water flow conditions were initiated with the oil-to-water injection ratio set to achieve a particular brine saturation along the two-phase relative permeability curve. This initial two-phase flow condition served as the "launch-off" for the three-phase saturation trajectory. These "launch-off" conditions were selected after reviewing the results from the oil-water test on sample 5. Three-phase flow was initiated by slowly increasing the gas flow rate to provide a pressure drop across the pressure measurement ports that was equal to about half of the measurement range of the pressure transmitter. The second three-phase flow condition on each DDI saturation trajectory was achieved by doubling the gas flow rate. The third measurement condition was set by halving both the brine and oil flow rates. Additional measurements were recorded after either doubling the gas rate or halving the oil and brine rates. This technique was orginally described by Oak et al.[17]

The relative permeability experimental apparatus was automated to provide for continuous flow and automated X-ray and microwave scanning for saturation determination during three-phase flow tests. Modifications to the equipment and details on the automated system are provided in appendix B of this report.

RESULTS

Sample Physical Characteristics

Clay and Minerals

Mineralogical characteristics of the fired 700-md Berea from XRD analysis were found to be very similar to those of the Bentheimer and Berea samples characterized during the FY89 experimental program. Clay mineral peaks were virtually absent on the X-ray diffraction clay minerals graph for the fired rock, as shown in figure 2, indicative of good clay stabilization. Iron sulfides, siderite, and ferroan dolomite were converted to hematite during the firing process, giving the rock a reddish color. Petrophysical properties of the rock from routine core analyses are shown in table 1.

Pore and Grain Size Distributions

The grain and pore size distributions from the computer-aided petrographic analysis for the sample were found to be well approximated by log-normal distribution functions. Grain and pore size distributions by number percent for the 700-md Berea are shown in figures 3 and 4 along with results for the 2,000-md Berea and 2,400-md Bentheimer sandstones studied during FY89. Note that the y-axis is a log scale while the x-axis is a normal probability scale. The Bentheimer sandstone had slightly larger grains than the two Berea samples, whereas the grain size distributions for the two Berea samples were almost identical. Figure 4 shows that the 700-md Berea sandstone had a greater number of pores of diameters smaller than 7 μm when compared to the other two samples .

Table 2 presents sizes corresponding to 84, 50, and 16 percentile values as well as σ results where

$$\ln\sigma = 0.5 \ln\left(\frac{d_{84}}{d_{16}}\right) \qquad (1)$$

Mercury intrusion porosimetry results for the 700-md Berea as well as the two other samples are shown in figure 5, which is a plot of log specific differential intrusion volume versus pore diameter. Like the log-normal distribution plot in figure 4, figure 5 shows the fairly narrow pore throat size distribution of Bentheimer compared to the two Bereas as well as the higher degree of microporosity exhibited by the 700-md Berea. Pore area and median pore diameter information for the 700-md Berea is given in table 1. Data for the other two samples are provided in reference 10. The mercury intrusion porosimetry tests were useful for characterizing pore size distributions including pores in the submicron range. The mercury data are very useful for discerning differences in microporosities when characteristics of different samples are compared.

Fluid Characteristics

The effluent from brine-saturated samples of the fired Berea rock was tested during intial brine injection tests and was found initially to be very basic. This high pH condition resulted due to having fired the rock at 1,000 ° C. High firing temperatures used to stabilize clay minerals are known[18] to convert calcite and dolomite to calcium and magnesium oxide. When neutral pH brine is then injected into the fired rock, the oxides change to hydroxides and the brine pH increases. The pH of the brine decreases as the number of pore volumes (PV) of injected brine increases. To evaluate the effect of the high pH on other rock parameters, resistivity measurements were recorded as one of the samples was initially flooded with brine. The initial resistivity for the sample was 6.2 ohm-m, and the pH of the effluent from the rock was 11.33. After allowing 2.3 PV of brine to flow through the rock, the pH dropped to 11.2, and the resistivity increased to 6.8 ohm-m. The pH dropped to 10.4 after an additional 54 PV of brine was pumped,

whereas the resistivity remained essentially constant. Tests were also conducted to evaluate the effect of the high pH brine on fluid interfacial tensions. Results from these tests are shown in table 3. Little difference was found between the interfacial tensions for oil (Soltrol 100) and the neutral or high pH brine. Therefore, the effect of the brine pH on capillary pressure and resistivity changes were considered to be negligible for the rock/fluid systems used in this investigation.

Capillary Pressure and Wettability

The following paragraphs summarize some of the key centrifuge capillary pressure and wettability results for the 700-md Berea that are presented in greater detail in another report.[10]

Amott Tests

Amott tests showed that the 700-md fired Berea had a greater affinity for the brine phase than for the oil phase. After 10 days in brine, a sample initially at residual brine saturation conditions (24% brine saturation) imbibed 0.34 PV of brine for a final brine saturation of 58%. A similar sample at residual oil saturation conditions was immersed in oil for 10 days but did not imbibe any oil.

CT images from scans taken of the plug at intervals of 1 minute, 15 minutes, and 60 hours as it imbibed brine in an Amott cell showed that the plug imbibed a significant volume of brine during the first minute of immersion. Brine was imbibed from both radial and axial directions. After initially imbibing significant quantities of brine, the imbibition process slowed considerably as continuity of oil channels to the upper plug surface was disrupted.

Centrifuge Capillary Pressure Tests

Wettability index results for the 700-md Berea are shown in table 4. Results for the other samples are in reference 10. Capillary pressure-saturation results from Hassler-Brunner and Rajan solutions were similar, and these similarities were reflected in the wettability index values.

High RPM, Long-Term Tests

Maximum capillary pressures developed during the high-RPM, long-term tests were 200 kPa (29 psi) during drainage and 262 kPa (38 psi) during imbibition cycles. Test results for the high-permeability Bentheimer sandstone indicated that the high capillary pressures induced during the high-RPM test drove residual saturation values below those that were measured in the laboratory during dynamic flow tests. The results from the high-RPM test were not considered descriptive of the sample characteristics with respect to the linear laboratory flow tests.

Low RPM Tests

Low-RPM, long-term test results for the two Berea sandstones showed hysteresis in both drainage and imbibition cycles when the first imbibition, first and second drainage curves from the long-duration (48 hr/point) tests were compared with the second imbibition and third drainage results from the short-duration (1 hr/point) tests. The shifts in the drainage curves appeared to be random, whereas the second imbibition cycle curves were offset from the first cycle curves in the direction of lower water saturation with more gentle curvature at capillary pressures up to about 21 kPa (3 psi), then converged with the first cycle curves as the residual oil saturation was approached.

Low RPM, Short-Term Tests

Capillary pressure-saturation curves and wettability indices from the low-RPM, short-term (1 hr/pt) were comparable with the those from low-RPM, longer duration tests for these samples.

Centrifuge/CT Scan Tests

CT scans of the 700-md Berea showed that the sample was very homogeneous and lacked bedding features. CT densities for the dry and brine saturated samples were 1,136 ± 22 and 1,577 ± 24 Houndsfield Units (HU),respectively.

Imbibition Process CT Results

Very little brine was imbibed at the outer edges of the 700-md Berea plug during the imbibition process for rotational speeds at or below 200 RPM, except at the outermost face of the plug, as shown in figure 6A. Figure 6B shows that significant imbibition occurred after rotation at 300 RPM. The figure shows the parabolic shape of the water distribution along a central plane through the plug. The transition from the region of high brine saturation to the region of high oil saturation was gradual. At higher rotational speeds, the front progressed toward the innermost plug face. After rotation at 800 RPM, the saturation throughout the plug appeared uniform and did not change significantly after rotation at 1,000 and 1,500 RPM.

Drainage Process CT Results

The variation in brine saturation changed gradually throughout the 700-md Berea plug during the drainage process, as shown in figures 6C and 6D. Significant changes in saturation occurred at speeds to 800 RPM. Uniform minor changes in saturations were noted from images taken after exposure to higher rotational speeds.

In summary, hysteresis effects were evident in each multiple-cycle centrifuge experiment. The primary effect of the cycle-dependent hysteresis for these samples was a reduction in the wettability index with successive drainage and imbibition cycles. Hysteresis effects were most pronounced for the portions

of the drainage capillary pressure curves for capillary pressures greater than about 4 psi and for water saturations less than about 25%. These portions of the drainage curves are influenced by pores which may be considered as microporosity. The data for capillary pressures lower than 3 psi were very repeatable and did not appear to be affected by hysteresis.

Relative Permeability Measurements

Oil-Water

Oil-water steady-state results for sample 4 (2,000 md Berea) data from two sets of drainage and imbibition cycles are shown in figure 7. The letter and number combinations in the legend such as w, d1 or o, i2 indicate the phase (water or oil) and drainage or imbibition cycle number. Although the saturation spread is very narrow, the relative permeability data from the four cycles all followed the same oil and water relative permeability trends and did not appear to be affected significantly by saturation history.

Unsteady-state oil-water relative permeability results for plugs 1, 2, and 3 (700-md Berea) are provided in tables 5 and 6. The results are also plotted in figure 8. Plug 3 results shown in figure 8 are for two imbibition cycles (a and b). Test characteristics were dissimilar in a number of areas. The confining pressure used for tests on plugs 1 and 2 was more than twice as great as that used on plug 3. As a result, the effective permeability values for plug 3 at each saturation were higher than those for plugs 1 and 2. The oil used in plug 3 tests was about 4 times as viscous as that used for plugs 1 and 2. Nonetheless, the relative permeability versus saturation results for each of the three plugs were very similar despite the differences in test procedures and conditions. Hysteresis effects did not appear to be significant in the test results.

Oil-water steady-state results for sample 5 (700-md fired Berea) are provided in table 7 and are shown in figure 9. After cleaning the sample at the end of the test, a leak was found in the the sample's epoxy resin jacket. Analysis of the data suggests that the leak may have occurred during the second drainage and imbibition cycles. Therefore, although relative permeability data for two drainage and imbibition cycles are provided in table 7, only the first drainage imbibition cycle results are considered representative. The water relative permeablity results from both sets of drainage and imbibition cycles all fell along the same relative permeability curve. Even if a small gas saturation existed within the rock, this result is still consistent with the commonly held premise that the water relative permeability is affected primarily by the water saturation alone. Resistance measurements were also recorded during the relative permeability experiment and are given in tables 7 and 8 and on figures 10 and 11. Figure 10 shows the path of the resistivity index results for the first drainage and imbibition cycle. Subsequent resistivity index results fell within the path formed by the first drainage and imbibition measurements. Figure 11 shows the power function fits to the data for each saturation cycle. Saturation exponent values (n) ranged from 1.46 to 1.88 for the particular fit equations, as shown in the graphs and in table 8. The best fit to the overall data

while forcing the curve to pass through the water saturation fraction =1, resistivity index =1 point yielded a saturation exponent value of 1.48.

Gas-Water

Gas-water steady-state relative permeability results for sample 6 (700-md fired Berea) from two drainage and one imbibition cycle are given in table 9 and are shown in figure 12. The gas-water results do not appear to show any appreciable cycle-dependent hysteresis effects beyond the obvious difference among nonwetting phase results during the first drainage and subsequent drainage and imbibition results.

Resistivity results for the sample are provided in table 10 and figure 13. Saturation exponent values ranged from 1.18 to 1.61 for the particular fit equations, as shown in the graph and in table 10. The best fit to the overall data while forcing the curve to pass through the water saturation fraction =1, resistivity index =1 point yielded a saturation exponent value of 1.42. This result is very similar to that determined from measurements recorded during the oil-water tests.

Three-Phase

The three-phase relative permeability tests have not been completed. The results of these tests will be reported in FY91 as soon as they are analyzed.

DISCUSSION

Capillary Pressure/Wettability Measurements

Hysteresis in drainage capillary pressure-saturation curves from tests in which multiple drainage and imbibition saturation cycles were performed did not appear to be consistent with any particular trend. The dominant trend in imbibition capillary pressure hysteresis was a shift of subsequent imbibition curves in the direction of lower brine saturation with more gentle curvature at low capillary pressures and convergence with previous curves at high brine saturations. This may be caused by changes in oil trapping with subsequent drainage/imbibition cycles. Wettability indices from subsequent imbibition/drainage cycles in this investigation were reduced, suggesting a decrease in water-wet characteristics with subsequent drainage/imbibition cycles. Trapping of the nonwetting phase is probably responsible to a greater degree than changes in wettability for the reduction in wettability index.

Except for one test, capillary pressures calculated from Hassler-Brunner and Rajan techniques and wettability indices calculated from the capillary pressure results were similar in each case. Rajan's model provided more consistent results for the rocks tested. The use of more than one model is preferred to ensure that data interpretation is correct.[19] Capillary pressure results for these high-permeability samples

did not appear to change significantly when time at each rotational speed was increased from 1 to 48 hr. Low-permeability samples may be affected differently, however.

CT scan images indicated that nonuniform saturation distributions resulted during centrifuge capillary pressure tests at capillary pressures intermediate between the end point saturation conditions. In designing a centrifuge capillary pressure test for a core sample, it is important to obtain sufficient measurements to describe the shape of the capillary pressure/saturation curves in the regions of high curvature.

Comparison of Two-Phase Results From This Investigation

Two-phase oil-water relative permeability curves from unsteady-state tests from this investigation were very similar even though the experiments were conducted by two different staff members on three different plugs using two different oils and under different confining pressure conditions. Two-phase water relative permeability versus water saturation curves were very similar from unsteady- and steady-state oil-water results and for gas-water steady-state results. Gas relative permeability versus water saturation curves from steady-state gas-water tests and oil relative permeability versus water saturation from unsteady-state tests fall almost on top of one another for water saturation fractions below about 0.70. The oil versus water saturation curves (drainage and imbibition) from the steady-state oil-water fall to the left (direction of lower water saturation) of the oil and gas versus water saturation curves from the other tests. As previously described, gas invasion may have influenced the two-phase steady-state oil curves. It was useful to have both unsteady- and steady-state relative permeability results to discern trends and to cross check the results.

Comparison of Two-Phase Results With Those From Other Investigations

Oak et. al.,[17, 20] Oak,[21] and Dria et al. [22] among others have presented comprehensive papers including their two- and three-phase relative permeability results for sandstone and dolomite rock samples. Figure 14 shows two-phase graphs of water, oil (water-oil imbibition), and gas (gas-liquid drainage) interpreted from Oak's[21] figures 5, 6, and 7, two-phase steady-state data from experiments on 200-, 800-, and 1,000 md fired Berea sandstone cores. Figure 15 shows graphs of model curves interpreted from figures 5, 6, and 7 of the Dria et al.[22] work with Baker dolomite under steady-state oil/brine/CO_2 flow conditions. The water relative permeability versus saturation curves from figures 14 and 15 are similar for the range of saturations considered. The oil and gas relative permeability versus water saturation curves are similar from the two figures for water saturation fractions below about 0.60. For water saturation fractions below 0.60, the steady state gas and unsteady-state oil relative permeability versus water saturation curves from this investigation are similar to those of figures 14 and 15. The steady-state oil relative permeability versus water saturation curves from this investigation fall slightly to the left (direction of lower water saturation) of the oil and gas curves in figures 14 and 15. The water permeabilities

from this investigation were higher than those in figures 14 and 15 for water saturation fractions below about 0.60. The high firing temperatures used in this investigation to stabilize clays may have left the samples with less microporosity and cleaner pores compared to the samples used by Oak and Dria et al.,[21-22] yielding the higher water relative permeabilities determined in this investigation.

CONCLUSIONS

The following observations and conclusions were made as a result of this experimental work.

From pore and grain size characterization:

1. Mercury intrusion porosimetry results are good for developing pore throat size distributions that include information on pores in the submicron range. The mercury data are very useful for discerning differences in microporosities when characteristics of different samples are compared.

From capillary pressure/wettability tests:

2. Hysteresis was evident in each multiple-cycle centrifuge capillary pressure experiment; primarily for measurents close to the residual saturations at high capillary pressures. The data for capillary pressures lower than 3 psi were very repeatable and did not appear to be significantly affected by hysteresis. The primary effect of cycle dependent hysteresis for these samples was a reduction in the wettability index with successive drainage and imbibition cycles.

3. Maximum capillary pressures induced during centrifuge capillary pressure tests should be limited to values similar to those occurring in the dynamic displacement process in order to yield representative capillary pressure/saturation and wettability information.

4. The use of more than one capillary pressure model is preferred to ensure that data interpretation is correct.

From relative permeability measurements:

5. Discernable hysteresis effects in the two-phase relative permeability results in high permeability Berea were essentially limited to the shift in nonwetting phase relative permeability versus saturation curves between the first drainage and imbibition tests in the direction of lower brine saturation for nonwetting phase saturations close to and less than the residual nonwetting phase saturation values.

6. Two-phase wetting phase relative permeability characteristics were consistent for unsteady- and steady-state oil-water or gas-water flow conditions.

7. It was useful to have both unsteady- and steady-state relative permeability results to discern trends and to cross check the results.

8. Non-wetting phase relative permeability results from unsteady-state tests were higher, than the steady-state valves at equivalent saturations. This may suggest higher recovery at water breakthrough and breakthrough when used in prediction of secondary recovery in high permeability rock such as this Berea if results are predicted from unsteady-state data.

9. Hysteresis in water relative permeability results was not significant which can be expected for a strongly water-wet rock.

10. Hysteresis in oil relative permeability results from oil-water tests was not significant at high oil saturations (greater than 45%). Performance prediction of secondary recovery for strongly water wet rocks should not be significantly affected by hysteresis high oil saturation conditions.

11. Similarity of water relative permeability results from both oil-water and gas-water tests and similarity of oil and gas relative permeability results from oil-water and gas-water tests are indicative of a strongly water-wet system.

ACKNOWLEDGMENTS

This work was performed for the U. S. Department of Energy (DOE) under Cooperative Agreement DEFC22-83FE60149. The authors thank Willis Waldorf, Ronald Masias, Michael Crocker, and Liviu Tomutsa of NIPER for their assistance in the laborabory with steady-state relative permeability, unsteady-state relative permeability, centrifuge capillary pressure, and CT scan measurements; to Kathy Burtus of NIPER for measuring IFTs; and to Ed Norman of NIPER for his contributions of designing and constructing the switches and electronic boards to automate the X-ray and microwave scanning operations. Appreciation is also extended to Shogo Suzuki of JAPEX for his assistance in analyzing some of the capillary pressure measurements, and to Jesus Betancourt of INTEVEP for his valuable contributions in the development of unsteady-state relative permeability and centrifuge capillary pressure computer programs to facilitate data analysis. Finally, we thank the NIPER management and other personnel who reviewed this manuscript, and Edith Allison, the DOE Project Manager.

REFERENCES

1. Anderson, W. Wettability Literature Survey -- Part 4. The Effects of Wettability on Capillary Pressure. J. Pet. Tech., Oct., 1887 pp. 1283-1300.

2. Anderson, W. Wettability Literature Survey -- Part 5. The Effects of Wettability on Relative Permeability. J. Pet. Tech., Nov.,1987 pp. 1453-1468.

3. Hawkins, J, and A. Bouchard. Reservoir Engineering Implications of Capillary Pressure and Relative Permeability Hysteresis. Pres. at the 1989 SCA Ann. Tech. Conf. SCA paper 8909.

4. Evrenos, A. and I. Comer. Numerical Simulation of Hysteretic Flow in Porous Media. Pres. at 44th Annual Fall Meeting of the Society of Petroleum Engineers of AIME, Denver, Sept. 28-Oct. 1, 1969. SPE paper no. 2693.

5. Szabo, M. New Methods for Measuring the Imbibition Capillary Pressure and Electrical Resistivity Curves by Centrifuge. Pres. at 45th Ann. Fall Meeting of the Society of Petroleum Engineers, Houston, Oct. 4-7, 1970. SPE paper 3038.

6. Batycky, J., F. McCaffery, P. Hodgins, and D. Fisher. Interpreting Relative Permeability and Wettability From Unsteady-State Displacement Measurements. SPEJ, June, 1981 pp. 296-308.

7. Longeron, D., M. Argaud, and J. Feraud. Effect of Overburden Pressure, Nature, and Microscopic Distribution of the Fluids on Electrical Properties of Rock Samples. To be presented at the 61st Annual Technical Conference and Exhibition of the Society of Petroleum Engineers, New Orleans, Oct. 5-8, 1986. SPE paper 15383.

8. Sinnokrot, A, H. Ramey Jr., and S. Marsden. Effect of Temperature Level Upon Capillary Pressure Curves. SPEJ, Mar., 1971, pp. 13-22.

9. Sanyal, S., H. Ramey Jr., and S. Marsden Jr.. The Effect of Temperature on Capillary Pressure Properties of Rocks. Proc. of the SPWLA Fourteenth Annual Logging Symposium, May 6-9, 1973.

10. Honarpour, M., D. Maloney, S. Suzuki, and L. Tomutsa. Investigation of Cycle Dependent Centrifuge Capillary Pressure and Wettability Index Behavior for Water-Wet High Permeability Sandstones. Pres. at the Fourth Annual SCA Technical Conference, Dallas Aug. 15-16, 1990. SCA paper 9006.

11. Maloney, D., M. Honarpour, and A. Brinkmeyer. The Effects of Rock Characteristics on Relative Permeability. Department of Energy Report No. NIPER-441, Jan. 1990. NTIS Order No., DE90000212.

12. Worthington, A. A Technique for Detecting Incomplete Saturation of Cores. J. Pet. Tech., Dec., 1978, pp. 1716-1717.

13. Hassler, G. and E. Brunner. Measurement of Capillary Pressures in Small Core Samples. Trans. AIME, v. 6, 1945, pp. 114-123.

14. Rajan, R. Theoretically Correct Analytical Solution for Calculating Capillary Pressure-Saturation From Centrifuge Experiments. Pres. at the SPWLA 27th Annual Logging Symposium, June, 1986.

15. Donaldson, E. and P. Lorenz. Wettability Determination and Its Effect on Recovery Efficiency. SPEJ, Mar., 1969, pp. 13-20.

16. Johnson, E., D. Bossler, and V. Naumann. Calculation of Relative Permeability from Displacement Experiments. Trans. AIME, Dec. 1958, pp. 68-74.

17. Oak, M., L. Baker, and D. Thomas. Three-Phase Relative Permeability of Berea Sandstone. Pres. at the SPE/DOE Enhanced Oil Recovery Symposium, Tulsa, Apr. 17-20, 1988.SPE/DOE paper 17370.

18. Shaw, J., P. Churcher, and B. Hawkins. The Effects of Firing on Berea Sandstone. Pres. at the SPE International Symposium on Oilfield Chemistry, Houston, Feb., 1989. SPE paper 18463.

19. Ruth, D. and S. Wong. Centrifuge Capillary Pressure Curves. J. Canadian Petroleum Technology, Vol. 29, No. 3, May-June, 1990 pp. 67-72.

20. Oak, M., and R. Ehrlich. A New X-ray Absorption Method for Measurement of Three-Phase Relative Permeability. SPE Reservoir Engineering, Feb., 1988 pp. 199-206.

21. Oak, M. Three-Phase Relative Permeability of Berea Sandstone. Pres. at the SPE/DOE 7th Symposium on Enhanced Oil Recovery, Tulsa Apr. 22-25, 1990. SPE paper SPE/DOE 20183.

22. Dria, D., G. Pope and K. Sepehrnoori. Three-Phase Gas/Oil/Brine Relative Permeabilities Measured Under Carbon Dioxide Flooding Conditions. Pres. at the DOE/SPE 7th Symp. on Enhanced Oil Recovery, Tulsa, OK Apr. 22-25, 1990. SPE/DOE paper 20184.

TABLE 1. - Characteristics of the 700-md fired Berea sandstone sample from routine core analysis and mercury intrusion porosimetry

Air permeability, md	630.0
Porosity, %	23.8
Total pore area, m^2/g	3.458
Median pore diameter, μm	16.8

TABLE 2. - Log-normal distribution function characteristics for Bentheimer and Berea sandstones

Permeability, md	Grain size, microns				Pore size, microns			
	d_{84}[1]	d_{50}	d_{16}	σ[2]	d_{84}	d_{50}	d_{16}	σ
Bentheimer, 2,400	290	203	140	1.439	181	105	66	1.656
Berea, 2,000	253	184	130	1.395	180	105	60	1.732
Berea, 700	253	177	124	1.428	160	94	64	1.581

[1]84% of the grains (by number) are smaller than d_{84}.

[2]$\ln\sigma = 0.5 \ln\left(\frac{d_{84}}{d_{16}}\right)$.

TABLE 3. - Characteristics of the brine and oil used in centrifuge capillary pressure and imbibition tests

Fluid(s)	7 pH brine	10.7 pH brine	Oil[1]	7 pH brine and oil	10.7 pH brine and oil
Viscosity, cP	1.01	1.01	1.1	—	—
Density, g/cm^3	1.005	1.005	0.739	—	—
IFT, mN/m	—	—	—	37	31

[1]Soltrol 100.

TABLE 4. - Wettability indices calculated from 700-md Berea capillary pressure results

Test	Wettability Indices	
	Hassler-Brunner	Rajan
Test 1 - Low RPM		
1st imb., 2nd drain. (48 hrs/point)	0.5	0.4
2nd imb., 3rd drain. (1 hr/point)	-0.1	0.1
Test 2 - Low RPM		
1st imb., 2nd drain.	Not used	0.2

TABLE 5. - Unsteady-state oil-water relative permeability results for Berea plugs 1 and 2

Oil viscosity, cP.....23.5
Brine viscosity, cP.....0.973
Confining pressure, psig.....800

Sample	k_{rw}	k_{ro}	s_w
Plug1 k_w 588 md @ s_w = 1.00	–	1.000	0.276
k_o 534 md @ s_w= 0.276	0.012	.332	.428
	.027	.348	.500
	.032	.275	.538
	.054	.173	.612
	.079	.138	.650
	.120	.045	.709
	.158	.005	.747
	.163	.003	.751
Plug 2 k_w = 630 md @ s_w = 1.000	–	1.000	.252
k_o = 534 md @ s_w = 0.252	.009	.509	.366
	.024	.483	.464
	.029	.230	.560
	.040	.174	.609
	.069	.083	.673
	.091	.065	.693
	.117	.031	.724
	.133	.018	.741
	.147	.005	.758

TABLE 6. - Unsteady -state oil-water results for Berea sandstone plug 3

Oil viscosity, cP.....93.5
Brine viscosity, cP.....0.973
Confining pressure, psig.....300

k_w = 700 md @ S_w = 1.000
k_o = 650 md @ S_w = 0.269

	kr_w	kr_o	S_w
Imbibition 1	–	1.000	0.269
	0.011	.606	.411
	.019	.401	.470
	.027	.347	.503
	.041	.278	.541
	.054	.258	.570
	.065	.190	.609
	.084	.129	.652
	.112	.085	.689
	.128	.047	.733
	.143	.019	.770
	.152	.013	.781
Imbibition 2	–	1.000	0.243
	.005	.387	.376
	.006	.337	.397
	.028	.269	.520
	.039	.311	.539
	.046	.187	.588
	.057	.142	.618
	.069	.141	.631
	.085	.133	.668

TABLE 7. - Oil-water relative permeabilty and resistivity data for sample 5 (700-md fired Berea)

Scan	Flow ratio w : nw	k_g, md	k_o, md	k_w, md	k_{rw}[1], fraction	k_{rg}[1], fraction	s_w fraction	R 4-wire	R_t/R_o
D1	0:1	679	–	–	–	–	–	–	–
51	1:0	–	–	643	–	–	1.000	387	1.00
2C	500:1	–	2.76	127	0.276	0.005	.793	528	1.36
5A	2:1	–	46	65	.142	.100	.584	658	1.70
6A	1:2	–	93	32	.070	.201	.537	817	2.11
7A	1:4	–	108	19	.041	.235	.501	940	2.43
8A	1:40	–	169	2.96	.006	.367	.398	1340	3.46
9A	1:500	–	353	0.49	.001	.767	.304	2106	5.49
10B	0:1	–	460	–	–	1.000	.197	5289	13.67
12	1:40	–	172	3.0	.0065	.374	.301	2806	7.23
13	1:4	–	97	17	.0370	.211	.510	1297	3.35
14	1:2	–	73	26	.0557	.158	.538	1150	2.97
15	2:1	–	31	43	.0937	.067	.549	866	2.24
16	15:1	–	6.0	63	.137	.013	.648	731	1.89
17	80:1	–	1.5	84	.183	.003	.723	659	1.70
18	200:1	–	0.62	88	.191	.0013	.737	634	1.64
19	1.0	–	–	91	.198	–	.735	620	1.60
- - - Oil permeability data below this line are questionable due to possible gas in the system - - -									
2J	80:1	–	1.2	68	.148	.0026	.690	709	1.83
3J	15:1	–	4.7	50	.108	.0102	.618	767	1.98
4J	2:1	–	22	31	.068	.048	.532	868	2.24
5J	1:2	–	60	22	.048	.131	.474	1047	2.71
6J	1:4	–	64	11	.025	.143	.458	1157	2.99
7J	1:40	–	118	2.1	.0046	.256	.367	1666	4.31
8J	0:100	–	218	–	–	.474	.287	2429	6.28
9J	1:40	–	137	2.4	.0052	.298	.366	1771	4.58
10J	1:40	–	64	11.4	.0248	.140	.467	1165	3.01
11J	1:2	–	46	16.5	.0359	.101	.473	1110	2.87
12J	2:1	–	18	25.4	.0552	.039	.508	877	2.27
13J	15:1	–	3.67	38.8	.0843	.008	.579	771	1.99

[1]Normalized with respect to k_o = 460 md at residual water saturation conditions.

TABLE 8. - Sample 5 oil-water resistivity results
$R_t//R_o = A/S_w^n$

Cycle	A	n	Correlation coefficient R
d1	0.85	1.60	0.993
i1	0.96	1.70	.993
d2	0.97	1.46	.996
i2	0.69	1.88	.992
fit using all data	1.00	1.48	–

TABLE 9. - Sample B72 gas-water data

Scan	Flow ratio w : nw	k_g, md	k_o, md	k_w, md	k_{rw}[1], fraction	k_{rg}[1], fraction	s_w fraction	R 4-wire	R_t/R_o
IDR	0:1	800	–	–	–	–	–	–	–
1	0:1	–	–	664	–	–	1.000	370	1.00
3	10:1	17.3	–	212	.335	.027	.575	484	1.31
5A	65:1	43.6	–	57.2	.091	.0690	.646	671	1.81
6	1500:1	214	–	10.6	.0168	.340	.477	1065	2.88
7	2000:1	260	–	8.8	.0139	.412	.453	1163	3.14
8	4000:1	282	–	6.20	.0098	.445	.419	1304	3.52
9	9000:1	426	–	3.60	.0057	.675	.352	1711	4.62
10	15000:1	489	–	2.50	.0040	.774	.322	1955	5.28
11B	1:0	632	–	–	–	1.000	.225	4019	10.86
12	17000:1	535	–	2.4	.00380	.847	.305	1843	4.98
13	8500:1	443	–	4	.00633	.701	.357	1530	4.14
14	4300:1	385	–	7	.0117	.609	.412	1322	3.57
15	2000:1	268	–	11	.0166	.424	.444	1039	2.81
16	1300:1	235	–	13	.0203	.372	.466	1064	2.88
17	520:1	139	–	18	.0291	.220	.516	933	2.52
18	180:1	78	–	31	.0495	.123	.584	801	2.16
19	90:1	50	–	52	.0816	.0785	.626	754	2.04
20	60:1	35	–	61	.0967	.0726	.682	709	1.92
21	40:1	0.4	–	68	.0910	.0554	.707	697	1.88
30	0.2:1	0.6	–	179	.283	.00101	.849	512	1.38
31	45:1	40	–	75	.119	.0633	.706	661	1.79
32	60:1	38	–	55	.087	.0601	.669	730	1.97
33	85:1	42	–	41	.0649	.0665	.599	805	2.18
34	180:1	79	–	33	.0516	.125	.607	795	2.15
35	580:1	129	–	16	.0256	.204	.496	966	2.61
36	1300:1	184	–	10.7	.0169	.291	.457	1112	3.01
37	2000:1	220	–	8.8	.0140	.348	.435	1199	3.24
39	8300:1	379	–	3.8	.0060	.500	.370	1565	4.23
40	15000:1	454	–	2.5	.00396	.718	.343	1832	4.95

[1]Normalized with respect to k_g = 632 md at residual water saturation conditions.

TABLE 10. - Sample 6 gas-water resistivity results
$R_t//R_o = A/S_w^n$

Cycle	A	n	Correlation coefficient R
d1	0.87	1.61	0.999
i1	1.19	1.18	.992
d2	1.10	1.34	.992
fit using all data	1.00	1.42	–

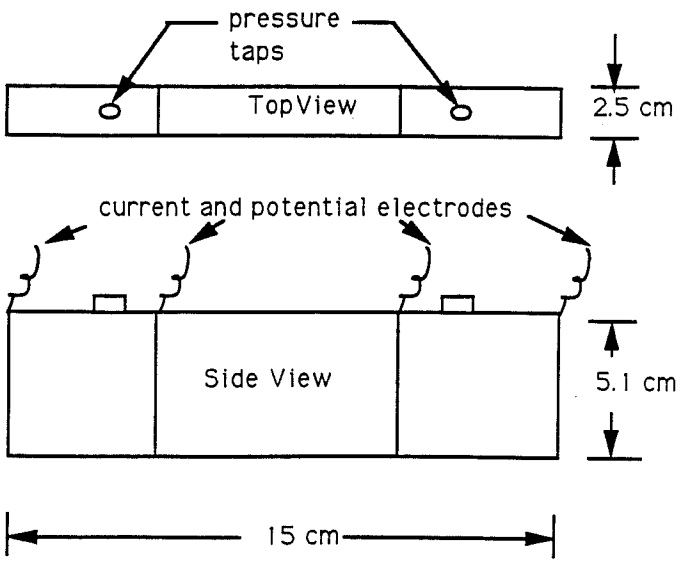

FIGURE 1. - Dimensions and electrode layout for rectangular samples 4, 5, and 6.

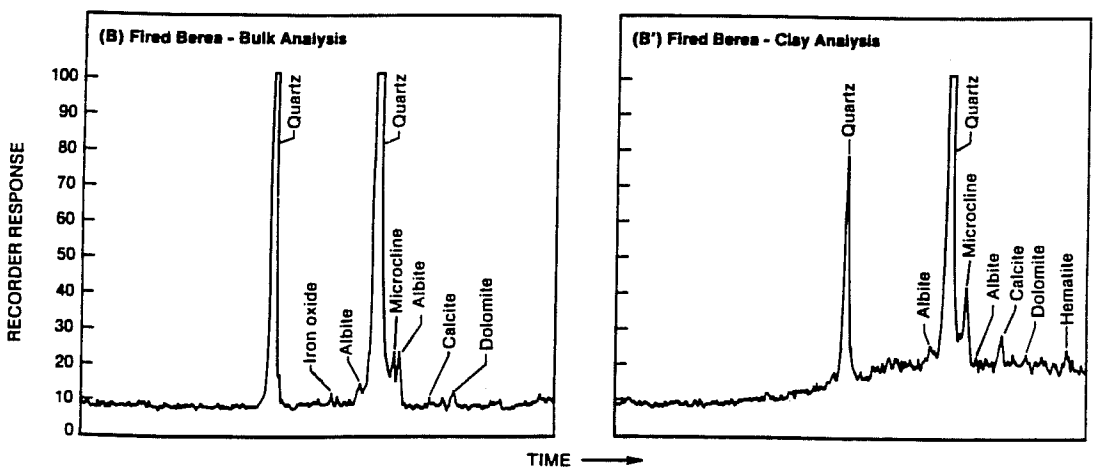

FIGURE 2. - X-ray diffraction bulk and clay analyses, 700-md fired Berea.

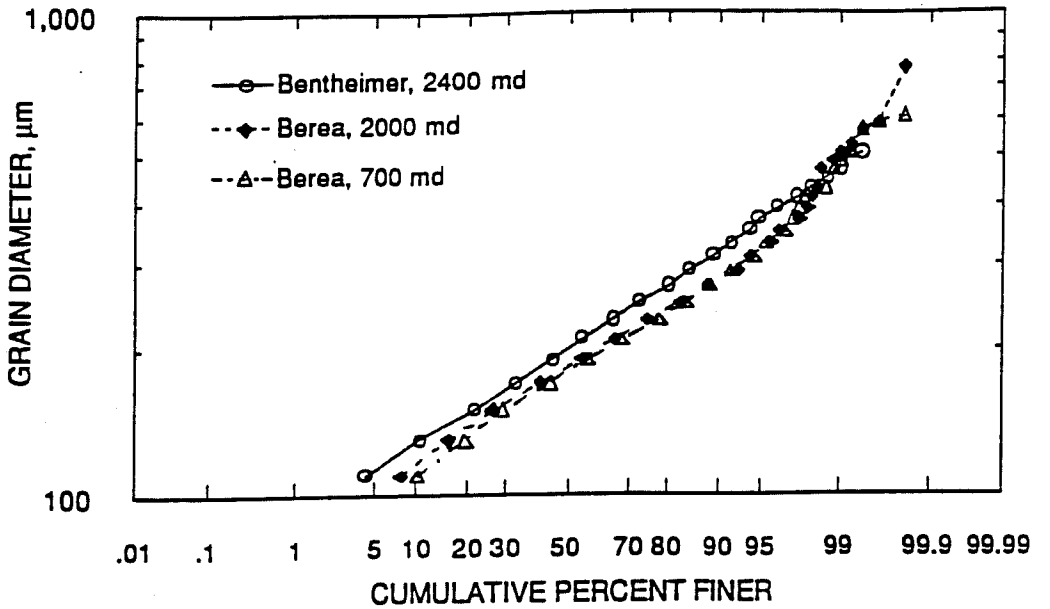

FIGURE 3. - Grain diameter distributions for fired Bentheimer and Berea samples from thin-section analyses.

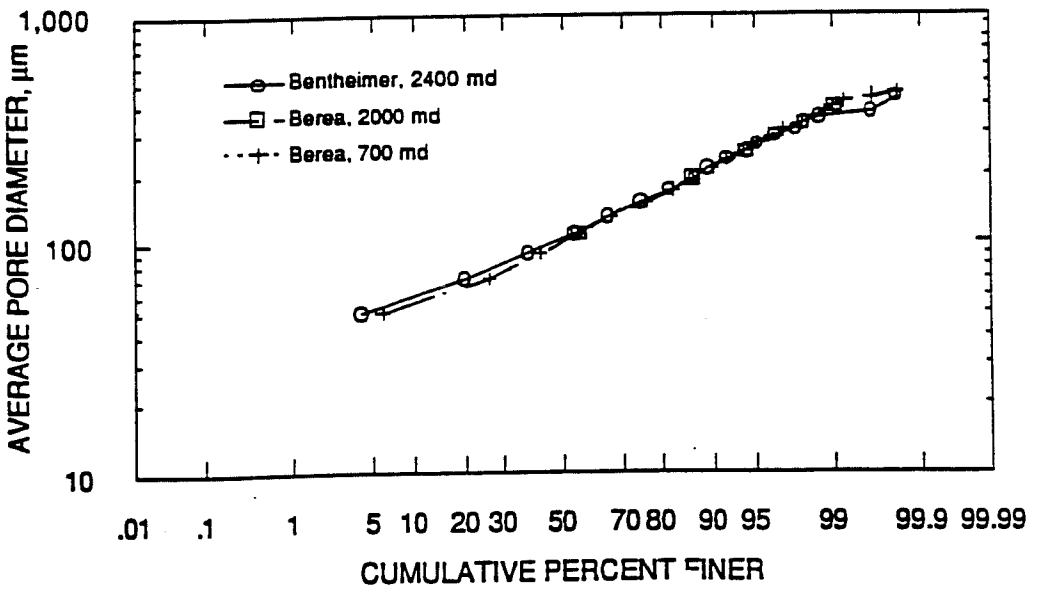

FIGURE 4. - Pore diameter distributions for fired Bentheimer and Berea samples from thin-section analyses.

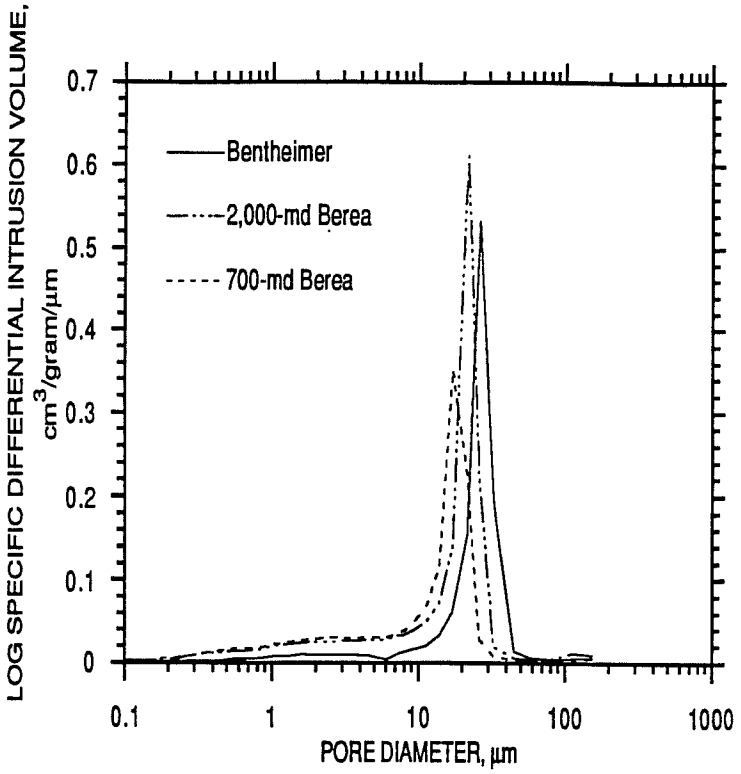

FIGURE 5. - Mercury intrusion porosimetry results for Bentheimer and Berea samples.

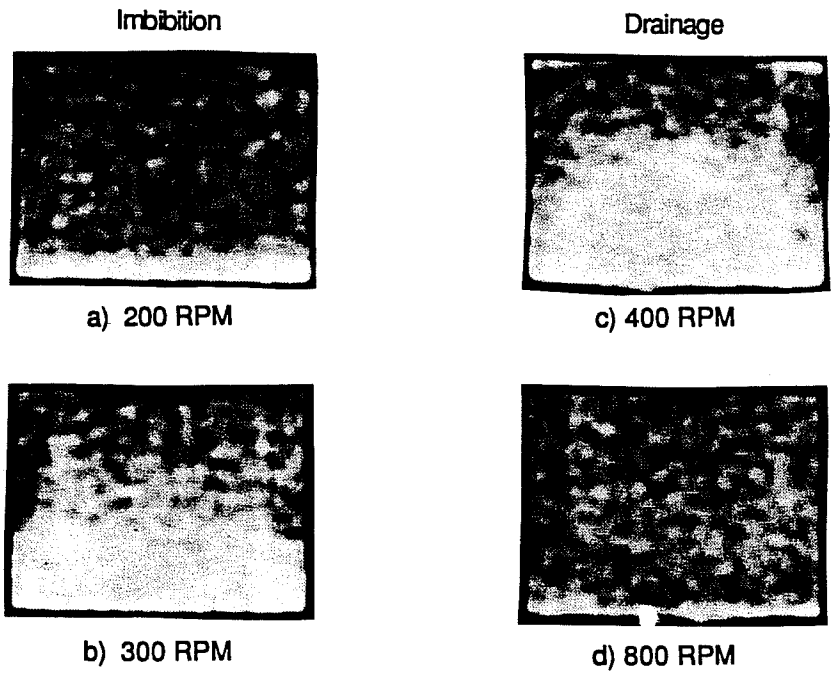

FIGURE 6. - CT images of the 700-md Berea during the 1st imbibition (left side) and 2nd drainage cycles showing brine (light) and oil (dark) distributions.

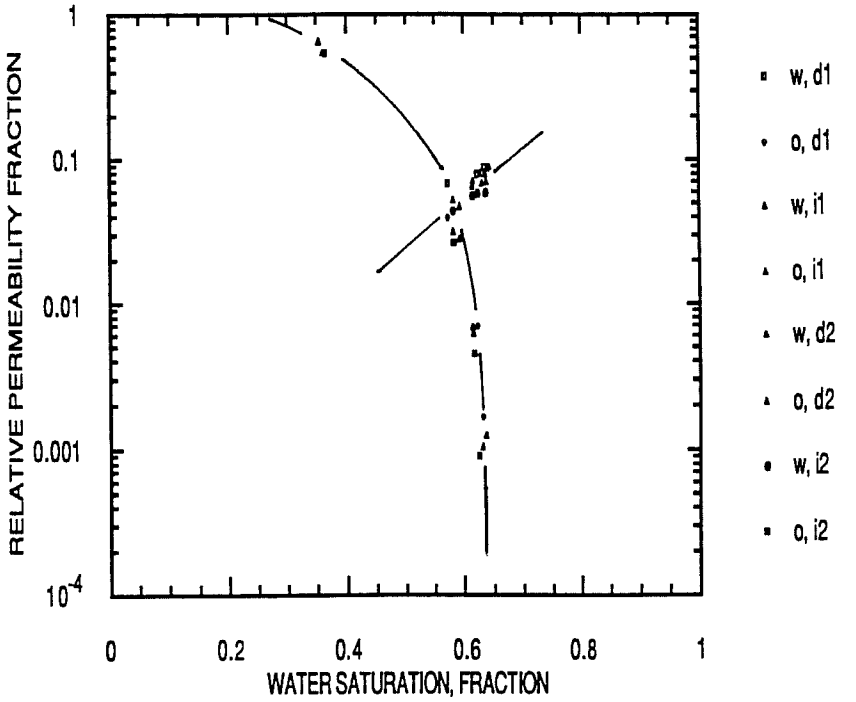

FIGURE 7. - Steady-state oil water results for sample 4 (2,000 millidarcy Berea sandstone). Results from 4 drainage and imbibition cycles are shown.

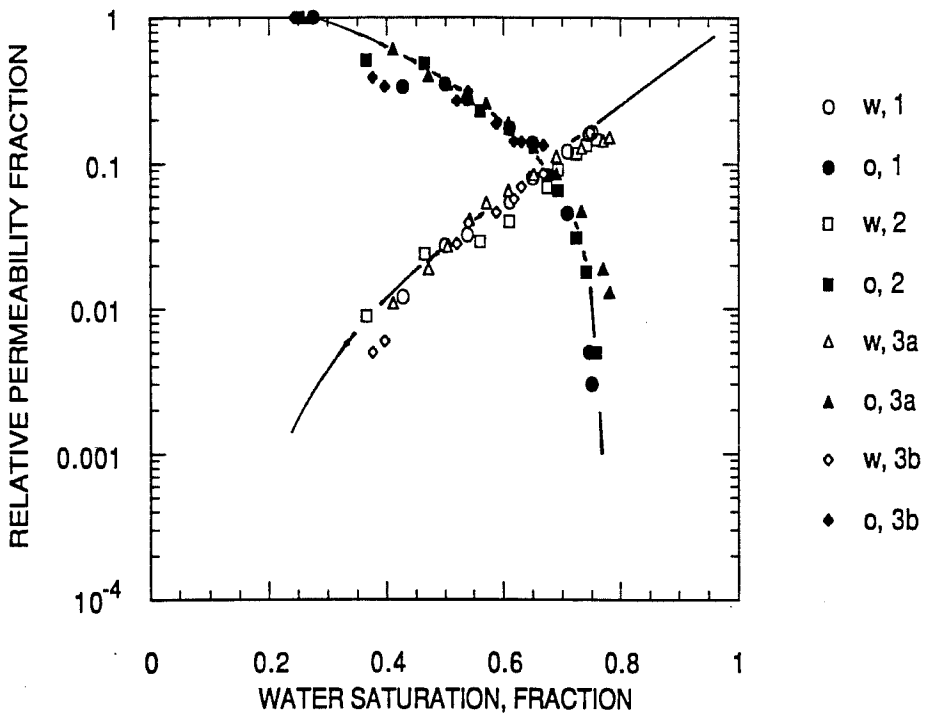

FIGURE 8. - Unsteady-state relative permeability results for 700-md Berea sandstone plugs 1, 2 and 3. Plug 1 and 2 were tested with 24 cP oil with 800 psig confining pressure. Plug 3 tests (2 imbibition cycles) were with 94 cP oil with 300 psig confining pressure.

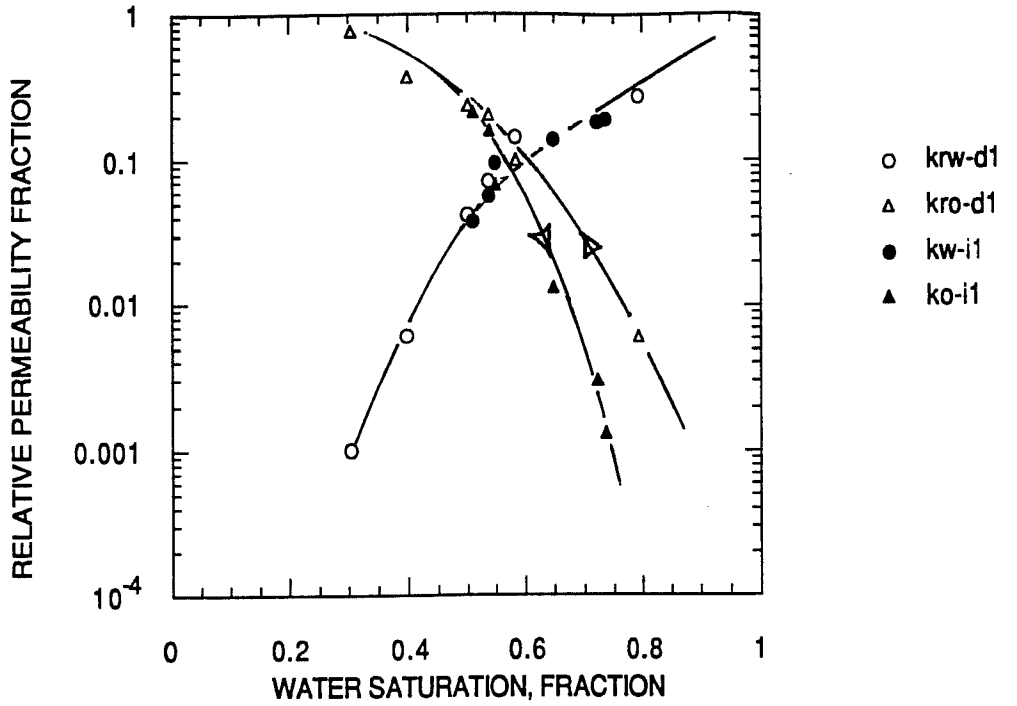

FIGURE 9. - Steady-state oil-water relative permeability results for sample 5 (700-md fired Berea). Oil viscosity = 1.2 cP.

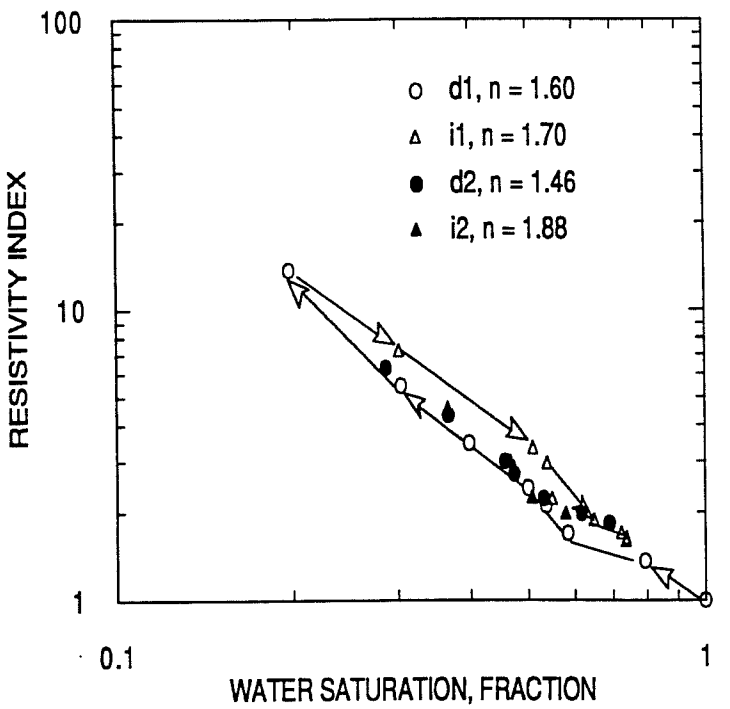

FIGURE 10. - Resistivity index results measured during the steady-state oil-water test on sample 5. The measurement path is shown.

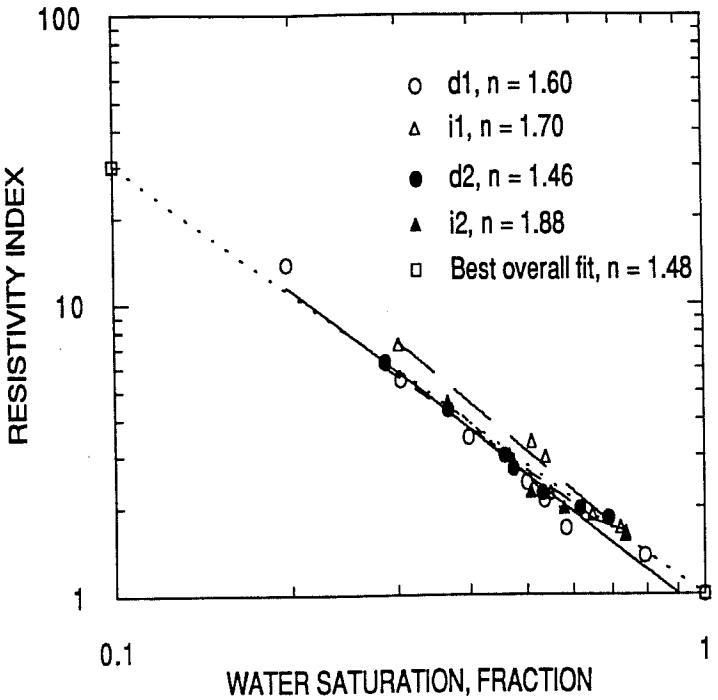

FIGURE 11. - Sample 5 resistivity index results showing curve fits and saturation exponents ('n').

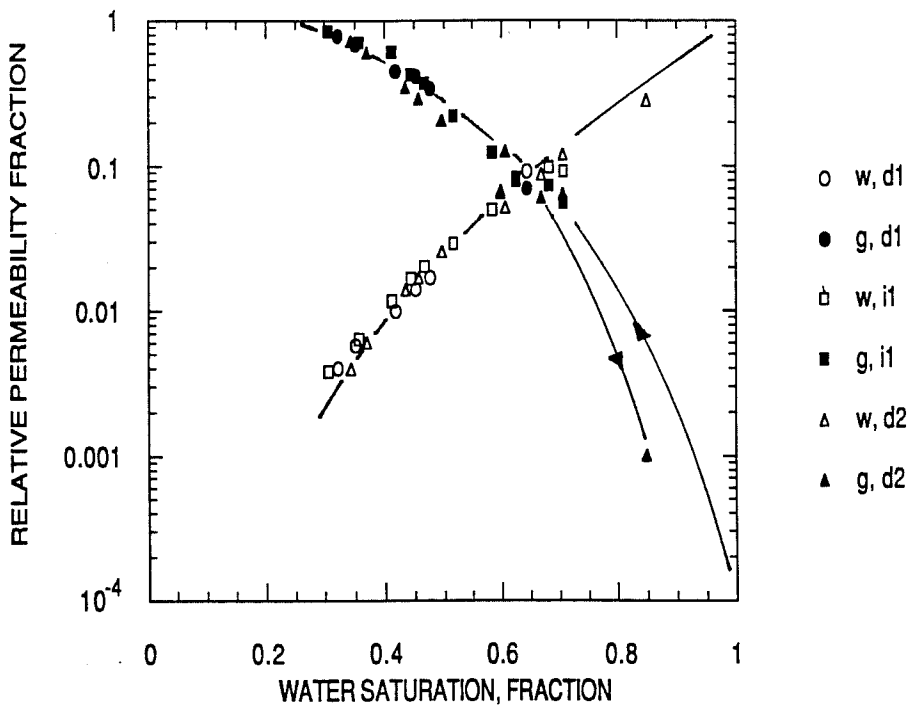

FIGURE 12. - Steady-state gas-water relative permeability results for sample 6 (700-md fired Berea).

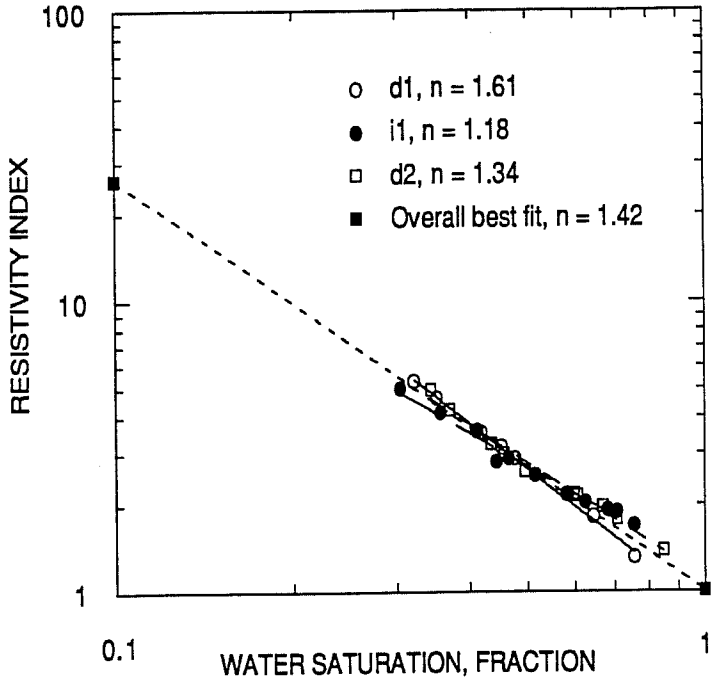

FIGURE 13. - Sample 6 resisitivity index results from measurements during steady-state gas-water tests. Curve fits and saturation exponents are also shown.

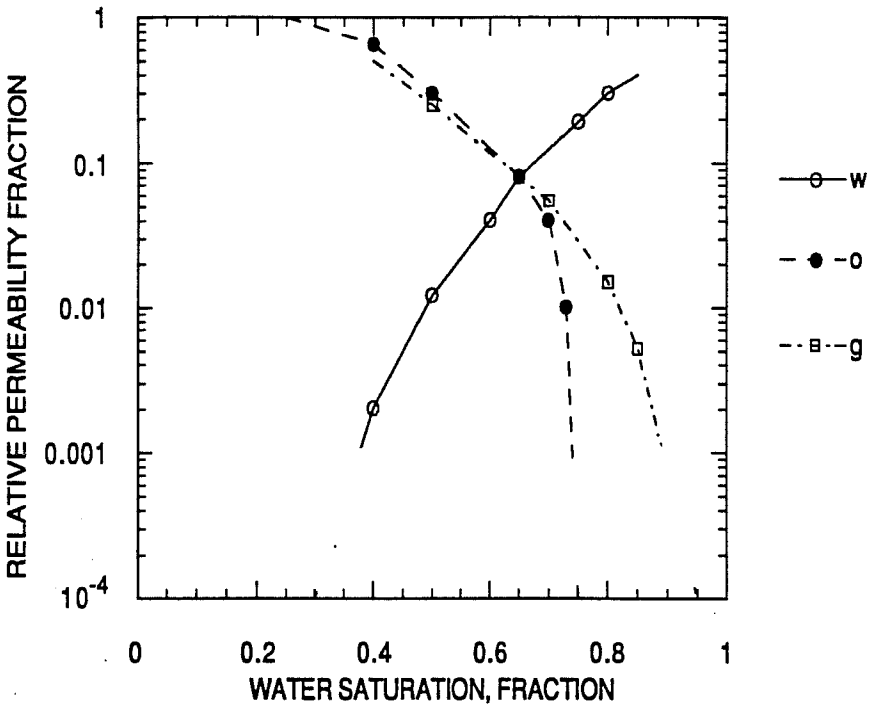

FIGURE 14. - Two-phase graphs of water, oil (water-oil imbibition), and gas (gas-liquid drainage) interpreted from Oak's[21] figures 5, 6, and 7.

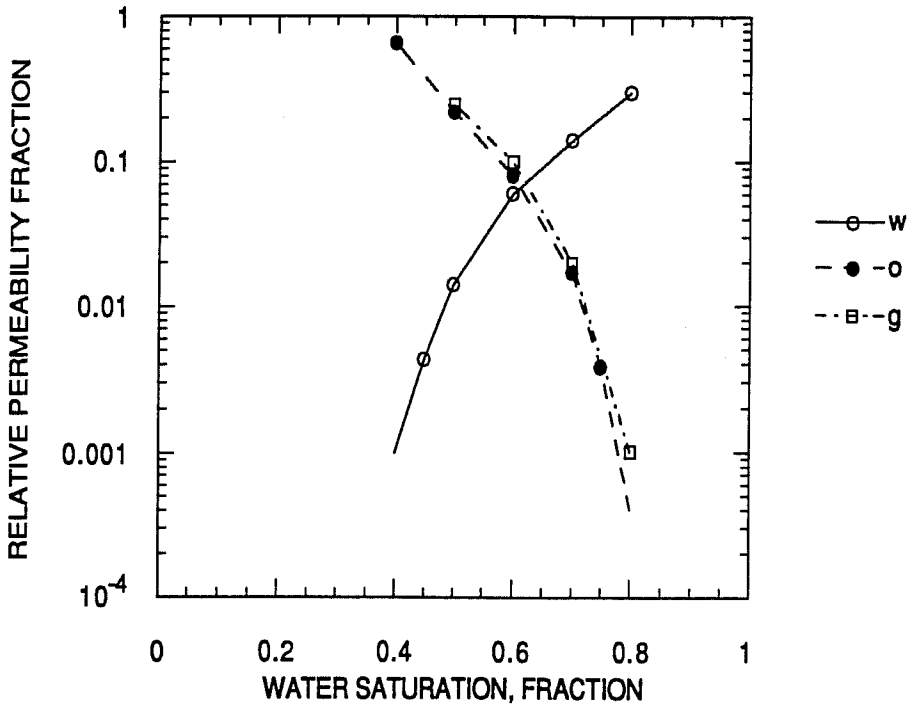

FIGURE 15. - Model curves interpeted from model results from figures 5, 6, and 7 of Dria et al.[22] work with Baker dolomite under steady-state oil/brine/CO_2 flow conditions.

APPENDIX A - TEMPERATURE EXPERIMENTS

Two experiments were conducted to evaluate changes in X-ray and microwave attenuation with temperature. Both experiments were conducted on 15 by 5 by 2.5 cm slabs of Berea sandstone.

The first experiment was conducted to evaluate whether changes in rock mineralogy or interstitial water could be sensed by the x-ray and microwave scanning equipment as the rock was dried at increasing temperatures. Prior to each test measurement, the rock was heated in an oven at the temperature of interest for 4 hours. The rock was then cooled in a dessicator to room temperature. Next, the rock was removed from the dessicator and was placed in an air tight plastic bag. The rock then was scanned by the X-ray and microwave. After each X-ray and microwave scan of the Berea, a standard with constant properties was also scanned. Scan results were normalized with respect to the results for the standard. Scans of the rock were taken after the rock was subjected to several temperatures from 22° to 1,000 °C. Essentially no detectable change in the rock's X-ray or microwave attenuation characteristics occurred due to exposure to temperatures within the test range.

The second experiment was conducted to evaluate changes in X-ray and microwave attenuation for a water saturated rock due to changes in temperature. The Berea slab used for this experiment was fired at 1,000 °C prior to the test and was then jacketed with epoxy resin. The rock was scanned with the X-ray and microwave under both dry and water saturated conditions at temperatures from 22° to 95 °C. In a manner similar to the previous temperature experiment, a standard was also scanned, allowing all results to be normalized with respect to the standard.

Temperature had no discernable effect on X-ray results within the range of temperatures measured, while attenuation of the microwave signal decreased as the temperature of the sample increased. The microwave results (natural log of the incident divided by the natural log of emergent microwave power, normalized with respect to the standard) essentially varied linearly with temperature such that the results for the brine saturated rock at 95 °C were 30% lower than those for the sample at the start of the temperature cycle (22 °C). The change in attenuation with temperature for the cooling cycle was less than that for the heating cycle.

Parsons[1] explained that microwave loss factors for water are dependent upon temperature, dissolved salts, and upon the particular laboratory experiment, but that in most cases, they should be second-order effects. The results from this experiment show that temperature has a significant effect on the attenuation characteristics of a brine saturated rock. Therefore, it is important to keep the test temperature constant while using microwave techniques for monitoring brine saturations during coreflood

experiments. Additionally, calibrations to relate microwave attenuation to brine saturations should be developed at the test temperature.

1. Parsons, R. Microwave Attenuation - A New Tool for Monitoring Saturations in Laboratory Flooding Expereiments. SPEJ, Aug. 1975, pp. 302 - 308.

APPENDIX B - NEW EQUIPMENT AND AUTOMATION

A GenRad 1692 RLC Digibridge was added to the system for resistance measurements. Code was developed to operate the RLC meter via the laboratory computer. A simple switch was built to provide for resistance measurements by either two-electrode or four-electrode methods.

Automation of the three phase relative permeability laboratory reached a new plateau during the project year. Additional hardware and software was added to the system in order to achieve a higher degree of automation and repeatability. A general schematic diagram of the automated experimental design is shown in figure B-1.

A 24-channel digital I/O board equipped with the 8255 Programmable Peripheral Interface Chip (INTEL) was used in the automation of the X-ray and microwave scanner. The board was placed in one of the slots in the back of the laboratory computer. The 24 I/O lines were configured into 20 output and 4 input lines for control and polling of the XRG 3100 X-ray generator and the microwave power supply. Each line is dedicated to a specific function including X-ray on/off, shutter open/close, X-ray power settings (KV and mA) and microwave power on/off. The custom electronic board to provide for automating the XRG 3100 settings and special switches to control the X-ray shutter and microwave beam on/off switch were designed and built in the NIPER electronics shop.

A typical scenario for using the automated system is for the user to enter injection rates selected for a multiphase flow experiment and the stabilization time for each measurement point. The system takes control from this point and at the specified time intervals measures and records resistance, pressures, X-ray and microwave scan data, calculates fluid saturations and permeabilities, and changes the injection rates for the next measurement point until the test is completed. The next higher level of automation involves including decision making logic within the program code to test for steady-state conditions and to adjust flowrates to optimally follow desired saturation trajectories. The objectives of attaining higher levels of automation are to save time, provide for uninterrupted testing, to increase repeatability of test results, and to minimize hysteresis effects on laboratory data.

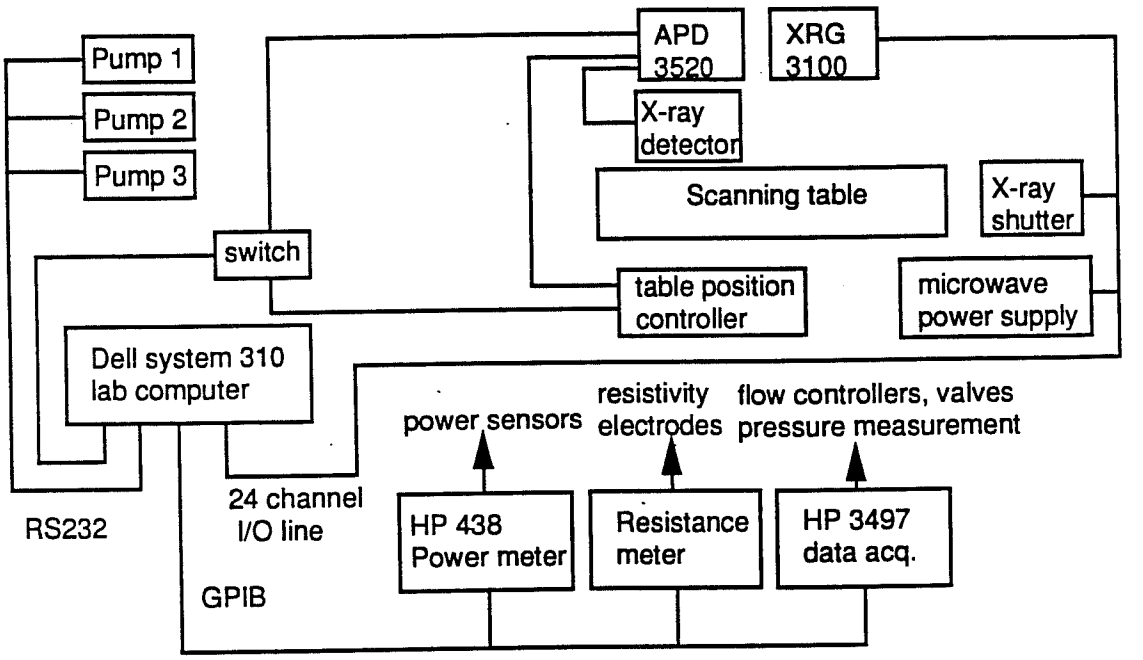

FIGURE B-1. - Generalized schematic of the input/output interconnections among the laboratory devices and measurement and control systems.